Available online at www.sciencedirect.com
ScienceDirect
Journal of Power Sources 176 (2008) 515–522
JOURNAL OF POWER SOURCES
www.elsevier.com/locate/jpowsour

Model-based control of cathode pressure and oxygen excess ratio of a PEM fuel cell system

Michael A. Danzer*, Jörg Wilhelm[1], Harald Aschemann, Eberhard P. Hofer

Department of Measurement, Control and Microtechnology, Ulm University, D-89081 Ulm, Germany

Available online 25 August 2007

Abstract

For PEM fuel cells supplied with air, pressure and flow control is a key requirement for an efficient and dynamic operation because fuel cells are in risk of starvation when the partial pressure of oxygen at the cathode falls below a critical level. To avoid oxygen starvation and, at the same time, to allow for a dynamic operation of the fuel cell system, both excess ratio of oxygen and cathode pressure need to be adjusted rapidly.

In this paper a model-based control structure is proposed that comprises a multivariable control of the cathode pressure p_C and the excess ratio of oxygen λ_{O_2} using the mass flow controller (MFC) and the outlet throttle as actuators. For both controlled variables appropriate desired values can be specified independently. As the derived dynamic model of the air supply system is nonlinear, advanced control techniques using differential flatness are applied.

Since the partial pressure of oxygen in the cathode flow field is a state variable that is hardly accessible by measurement, a tracking observer is employed to estimate this pressure using the measured air pressure at the outlet throttle. Thereby, the observer enables the control system to detect both temporary shortages of oxygen and peak pressures at the cathode and to counteract accordingly.

Keywords: Starvation prevention; Pressure control; Air flow control; Pressure observation; Fuel cell dynamics

1. Introduction

Fuel cells (FC) are energy converters that are not subject to the Carnot cycle and can, therefore, provide electrical power and heat efficiently, even in the part-load range. In case of hydrogen as fuel no direct emissions occur.

In automotive and several niche transportation applications FCs act as propulsion engine or as auxiliary power unit. In stationary applications fuel cells are utilised as combined heat and power plants or as uninterruptible power supplies.

The prevalent type of fuel cell is the polymer electrolyte membrane fuel cell (PEMFC), which is characterised by a high power density and a low operating range with temperatures from 0 to 90 °C. In both applications mentioned, a dynamic and efficient performance is required due to varying operating conditions and an operation with alternating loads. The power response of the fuel cell system depends mainly on the interaction of the fuel cell stack itself and the necessary peripheral components like air and fuel supply, flow and pressure control, heat and water management. Hence, the control objectives are to maintain efficiency and to avoid degradation by guaranteeing appropriate temperature, humidity and partial pressures of the reactants across the electrode.

Flow and pressure control in particular is a key requirement for an efficient and dynamic performance of the PEMFC [6]. Fuel cells are in risk of starvation during high current demand (see Fig. 2) and fast load changes (see Fig. 1) [12]. Starvation comes along with a drop in partial pressure of oxygen and occurs when more gas molecules react than are fed to the active surface.

The mass flow $\dot{m}$air at the inlet of the cathode is usually provided by a feedforward control proportional to the actual current, according to Faraday's Law

$$\dot{m}_{\mathrm{air,in}} = \lambda_{O_2} \frac{\dot{m}_{O_2,\mathrm{react}}}{y_{O_2}} = \lambda_{O_2} \frac{N\, M_{O_2}\, I_{\mathrm{FC}}}{y_{O_2}\, z\, F}, \tag{1}$$

with the mass fraction of oxygen in air y_{O_2} and the excess ratio $\lambda_{O_2} = \dot{m}_{O_2,\mathrm{in}}/\dot{m}_{O_2,\mathrm{react}}$. As can be seen in Fig. 1, this feedforward control of the mass flow leads to a temporary undersupply

* Corresponding author. Tel.: +49 731 5026325
E-mail address: michael.danzer@uni-ulm.de (M.A. Danzer).
[1] Present address: Forschungszentrum Jülich, Institute for Materials and Processes in Energy Systems (IWV-3), D-52425 Jülich, Germany.

0378-7753/$ – see front matter © 2007 Elsevier B.V. All rights reserved.
doi:10.1016/j.jpowsour.2007.08.049

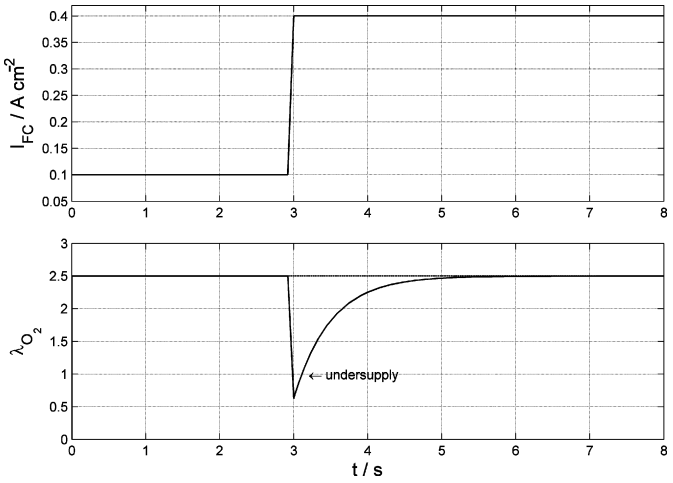

Fig. 1. Excess ratio of oxygen and cathode pressure at current step.

with $\lambda_{O_2} < 1$. Due to the time constant of the supply system oxygen cannot be replenished fast enough.

Diffusion is a limiting factor in the case of high current density. Reactant concentration drops and concentration overvoltage increases significantly due to both high reactant consumption and head loss at high flow rate. The limiting current with every incoming molecule reacting immediately is referred to as I_{lim}. The limiting current leads to a steep decline in voltage in the *IV* characteristics at high currents (Fig. 2).

The *I–V* characteristics can be described theoretically (2) by the equilibrium voltage via the Nernst equation and additional loss terms in terms of overvoltages η_i [1]. The fuel cell voltage U_{FC} is a function of the fuel cell current I_{FC}, the stack temperature T_{FC}, the partial pressures p_{O_2} and p_{H_2} of the reactants at the electrodes, the porosity ϵ of the gas diffusion layer and the conductivity κ of the membrane

$$U_{\text{FC}}(I_{\text{FC}}, \underline{x}) = U_{\text{eq}} - \eta_{\text{act}} - \eta_{\text{conc}} - \eta_{\text{ohm}}, \tag{2}$$

with $\underline{x} = [T_{\text{FC}}, p_{O_2}, p_{H_2}, \epsilon, \kappa]^{\text{T}}$.

Related to the partial pressures of the reactants, two effects are important. First, decreasing partial pressures lead to a lower voltage level all over the *I–V* characteristics due to an increased concentration overvoltage. Second, the limiting current I_{lim} depends on the stack temperature, the reactant partial pressure and the porosity of the gas diffusion layer

$$I_{\text{lim}} = f(p, T, \epsilon). \tag{3}$$

If the partial pressures of the reactants drops, I_{lim} decreases and the *I–V* characteristics is deformed towards smaller currents. This reduces the available operating range. A drop in partial pressures at high currents puts a crucial risk to the cell. If the limiting current falls below the actual fuel cell current, the cell polarity gets reversed. This effect harms the cell by damaging the catalyser.

In order to prevent starvation, feedforward control of the air mass flow and pressure control at the outlet of the system are insufficient. As will be shown in the following, multivariable feedback control of the cathode pressure p_{C} and the excess ratio of oxygen λ_{O_2} using the mass flow controller (MFC) and the outlet throttle as actuators, complies with the requirements. Since the flow dynamics is nonlinear, as described in Section 3, nonlinear model-based pressure control is proposed in Section 5. Here, a first problem arises: the partial pressure of oxygen at the electrode is an unknown inner state variable and hardly accessible by measurements. Hence, an observer is employed to estimate this pressure using the measured pressure at the outlet throttle of the fuel cell system. Thereby, the dynamic observer allows for detecting temporary shortages or peak pressures at the electrode and enables the control system to counteract accordingly.

2. Fuel cell subsystem

The core of the test rig is given by a fuel cell stack as depicted in Fig. 3 from the centre of solar energy and hydrogen research (ZSW) in Ulm with 25 cells and a nominal power of 800 W_{el}. The air supply subsystem of the fuel cell comprises the flow channels of the fuel cells and all the peripheral components required to supply air and to remove water and exhaust. The test rig is supplied with dry compressed air with a maximum of 2 bar_{abs}. The air is humidified by a dew point humidifier. The air flow fed to the stack is controlled by a mass flow controller. The supply manifold between the MFC and the stack consists of pipes and connections. Another manifold connects the outlet of the stack with the outlet throttle that is used for controlling the cathode pressure.

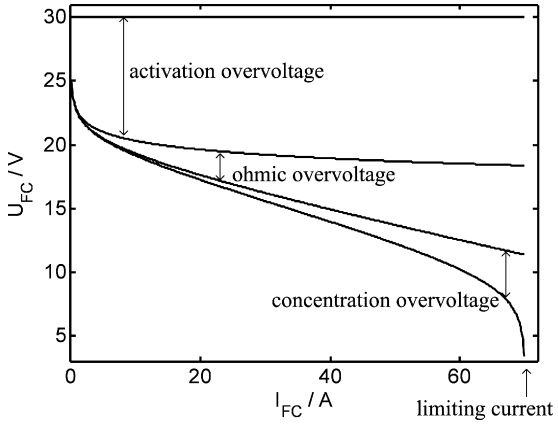

Fig. 2. *I–V* characteristics with limiting current.

Fig. 3. Fuel cell stack.

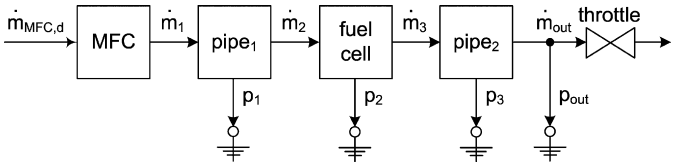

Fig. 4. Structure of the gas supply subsystem.

In the following, the supply pressure at the MFC is assumed as constant. Modelling focuses on the system illustrated in the block diagram in Fig. 4.

3. Dynamic model of the air supply system

Modelling the air supply system aims at describing the interaction of the mass flow controller and the outlet throttle with the cathode pressure p_C and the excess ratio of oxygen λ_{O_2} dynamically. The model is achieved by developing an equivalent circuit diagram for the pneumatic system using analogies to electrical systems [10].

3.1. Lumped pneumatic model

Pneumatic resistances and capacities form lumped parameters of the model. A pneumatic resistance describes the friction losses of a gas flow and a capacity represents the ability of a component to store mass [9]. Pipes, manifolds, throttles and flow channels of the fuel cell stack can be modelled by using such pneumatic resistances and capacities. In the following these subsystems as well as the whole equivalent circuit including the mass flow controller will be described mathematically.

3.2. Model of the mass flow controller

As described in (1) the desired air mass flow to operate the system is calculated using Faraday's Law

$$\dot{m}_{\mathrm{MFC,d}} = \frac{\lambda_{O_2}\, N\, M_{O_2}\, I_{\mathrm{FC}}}{y_{O_2}\, z\, F} \tag{4}$$

Since the MFC does not react instantaneously on a change in the desired mass flow $\dot{m}_{\mathrm{MFC,d}}$, this characteristic can be described as a first order lag element with the time constant τ

$$\tau \frac{\mathrm{d}}{\mathrm{d}t}\dot{m}_{\mathrm{MFC}} + \dot{m}_{\mathrm{MFC}} = \dot{m}_{\mathrm{MFC,d}}. \tag{5}$$

If the pressure p_1 at the outlet of the MFC rises, the effective mass flow $\dot{m}_1$ decreases. If p_1 equals the supply pressure $p_{\max}$ the mass flow saturates which is described by the saturation function

$$\dot{m}_1 = \tanh\{a\,(p_1 - p_{\max})\}\dot{m}_{\mathrm{MFC}}. \tag{6}$$

3.3. Model of the manifold

There are two manifolds in the system. The inlet manifold between the MFC and the fuel cell and the outlet manifold between the fuel cell and the throttle. The simplest model of a manifold or a pipe is a pneumatic capacity and a pneumatic resistance in parallel (Fig. 5). Generally, there are two borderline cases of flow, laminar [10] and turbulent [4] flow. Accordingly, laminar resistances R_{lam} and turbulent resistances R_{turb} have to be distinguished. In the case of laminar flow the mass flow is proportional to the pressure drop at the resistance

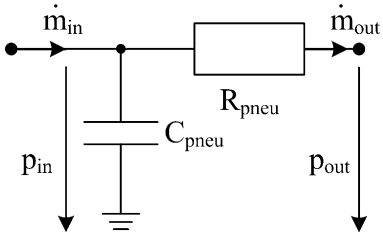

Fig. 5. Model of the manifold.

$$\Delta p = R_{\mathrm{lam}}\dot{m}. \tag{7}$$

In the case of turbulent flow the mass flow is proportional to the root of the pressure drop

$$\sqrt{\Delta p} = K_{\mathrm{turb}}\dot{m}, \tag{8}$$

with the constant parameter K_{turb} and the pressure dependent turbulent flow resistance

$$R_{\mathrm{turb}} = K_{\mathrm{turb}}\sqrt{\Delta p}. \tag{9}$$

Since laminar and turbulent flow are borderline cases, the pneumatic resistance of a pipe can also be modelled as a series of a laminar and a turbulent resistance (Fig. 6).

3.4. Model of the fuel cell stack

In analogy to the manifold model the fuel cell stack model (Fig. 7) consists of a laminar and a turbulent resistance and a capacity. The resistance results from the friction losses of the gas flow through the flow fields. The capacity results from the storage volume of the flow fields and the gas diffusion layer. The FC model differs in the configuration of the components, which is founded on the results of the parameter identification (cf. Section 4). Furthermore, the change in mass flow at the electrode has to be taken into consideration. The effective mass flow

$$\dot{m}_{\mathrm{eff}} = \dot{m}_{\mathrm{r}} + \dot{m}_{\mathrm{mem}} + \dot{m}_{\mathrm{H_2O}} \tag{10}$$

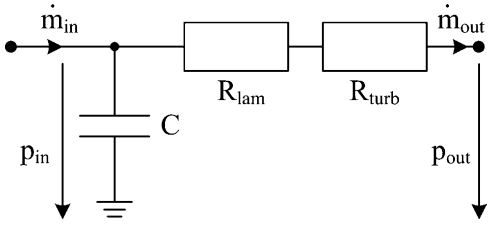

Fig. 6. Equivalent circuit of the inlet and outlet manifold.

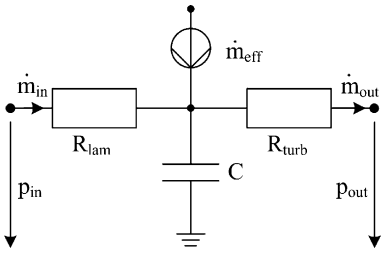

Fig. 7. Equivalent circuit of the fuel cell stack.

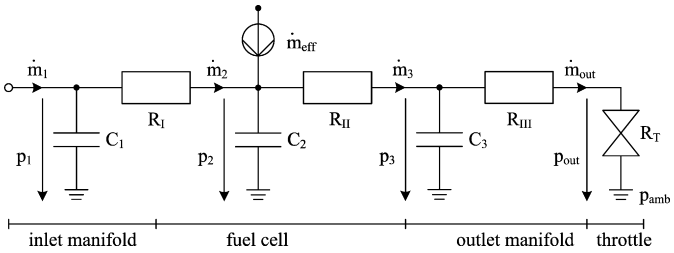

Fig. 8. Equivalent circuit of the air supply system.

is modelled as a source in the equivalent circuit. The effective mass flow consists of the mass flow $\dot{m}_r$ of the reaction at the cathode side, the mass transport $\dot{m}_{mem}$ through the membrane and the mass flow $\dot{m}_{H_2O}$ of water coming from the humidifier. The mass flow of the reaction

$$\dot{m}_r = \left(\frac{M_{H_2O}}{z_{H_2O}} - \frac{M_{O_2}}{z_{O_2}} \right) \frac{NI_{FC}}{F} \tag{11}$$

comprises the creation of water and the consumption of oxygen at the current I_{FC}. The mass flow

$$\dot{m}_{mem} = \dot{m}_{drag} - \dot{m}_{diff} \tag{12}$$

describes the water transport through the membrane caused by the electro-osmotic drag ($\dot{m}_{drag}$) and by back-diffusion ($\dot{m}_{diff}$). The description of $\dot{m}_{drag}$ and $\dot{m}_{diff}$ can be found in Refs. [7] and [2]. The derivation of the amount of water $\dot{m}_{H_2O}$ carried in by the humidifier can be seen in Ref. [13]. It results in

$$\dot{m}_{H_2O} = \frac{R_{air}}{R_{H_2O}} \frac{p_{sat}(T_{hum})}{p_C - p_{sat}(T_{hum})} \tag{13}$$

with the gas constants R_{air}, R_{H_2O} and the saturation pressure p_{sat} at the temperature T_{hum} of the humidifier.

3.5. Model of the throttle

The throttle at the outlet is modelled by a turbulent resistance [4]. The throttle resistance R_T can be changed by varying the opening area A_T. The mass flow through the throttle is calculated by

$$\dot{m}_{out} = \frac{p_{out}}{R_T} = \mu A_T \sqrt{\frac{2}{\rho}} \sqrt{p_{out}}. \tag{14}$$

3.6. Model of the air supply system

Connecting all subsystems to the overall model of the air supply system leads to the equivalent circuit in Fig. 8 with the combined resistances

$$R_I = R_{lam1} + R_{turb1} + R_{lam2},$$
$$R_{II} = R_{turb2} \quad \text{and} \quad R_{III} = R_{lam3} + R_{turb3}.$$

The dynamics of the pneumatic system is described by a set of oridnary first order differential equations

$$\dot{m}_1 = C_1 \dot{p}_1 + \frac{p_1 - p_2}{R_I} \tag{15}$$

$$\frac{p_1 - p_2}{R_I} = C_2 \dot{p}_2 + \frac{p_2 - p_3}{R_{II}} + \dot{m}_{eff} \tag{16}$$

$$\frac{p_2 - p_3}{R_{II}} = C_3 \dot{p}_3 + \frac{p_3}{R_{III} + R_T}. \tag{17}$$

These differential Eqs. (15)–(17) together with the equations of the MFC (5) and (6) describe the entire system dynamics of the air supply system.

4. Parameter identification

In Ref. [13] measurements were done to identify the parameters $C_1, C_2, C_3, R_I, R_{II}$ and R_{III} of the air supply model for a wide range of mass flows. The air mass flow through the system was changed stepwise from a minimum of 0.5 $g\,s^{-1}$ to a maximum of 2 $g\,s^{-1}$. The parameters for each subsystem were obtained from the measurements by using the Nelder–Mead algorithm for parameter optimisation [5]. Inputs to the algorithm are the measured pressure values $\underline{y}_{mea}$, the actual mass flow $\dot{m}_{in}$ and the derived model description in form of discretised differential equations. With these finite difference equations the model values $\underline{y}_{mod}$ are calculated. The algorithm then calculates the optimal parameter vector

$$\underline{\theta} = [C_1, C_2, C_3, R_{lam1}, R_{lam2}, R_{lam3}, K_{turb1}, K_{turb2}, K_{turb3}]^T$$

by minimizing the quadratic error

$$e = (\underline{y}_{mea} - \underline{y}_{mod})^2 \tag{18}$$

between the measured values and the model values.

As an example of an identified subsystem, in Fig. 9 the results from the parameter identification for the fuel cell stack can be seen. Here the measured pressure values $p_{2,mea}$ and the simulated model values $p_{2,mod}$ are compared.

By parameter identification the values of the parameters for the MFC (τ), the capacities (C_1, C_2, C_3), the laminar resistances (R_{lam1}, R_{lam2}, R_{lam3}) and the constant factors for the turbulent resistances (K_{turb1}, K_{turb2}, K_{turb3}) were determined as can be seen in Table 1.

The last missing parameter in Fig. 8 is the throttle resistance R_T. As described above the throttle is modelled by a turbulent

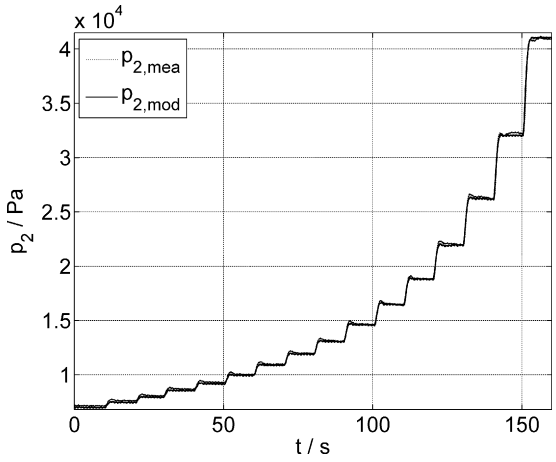

Fig. 9. Comparison between measured values for p_2 and model values.

resistance. By combining (8) and (9) you get

$$R_T = K_T^2 \dot{m}_{out} \tag{19}$$

The factor K_T depends on the throttle opening area A_T, which can be changed by varying the control voltage V_T of the throttle. The throttle resistance in (19) depends on the mass flow $\dot{m}_{out}$ through the throttle and the control voltage V_T. In the model the value for the throttle resistance R_T is derived from a characteristic map $R_T = f(\dot{m}_{out}, V_T)$, which can be seen in Ref. [13].

5. Nonlinear model-based control

The main control objectives are obtaining high overall efficiency and avoiding starvation. As for the air supply system of the fuel cell, the multivariable control involves set-point control of the cathode pressure $p_C = p_2$ and set-point control of the oxygen excess ratio λ_{O_2}. Accordingly, the control outputs are chosen as $y_1 = p_2$ and $y_2 = \lambda_{O_2}$. The subsystem offers two means that have an effect on the pressure and the excess ratio: the MFC at the inlet and the outlet throttle. Thus, the control inputs are the desired mass flow $\dot{m}_{MFC,d}$ and the flow resistance R_T of the throttle, which refers to the cross sectional area (cf. (14)) and the control voltage, respectively. Here, the integrated MFC represents a fast underlying control loop. The state variables of

Table 1
Identified parameters

Parameter	Value
τ	0.495 s
C_1	2.17×10^{-9} m s^2
C_2	4.46×10^{-8} m s^2
C_3	1.25×10^{-9} m s^2
R_{lam1}	6.94×10^6 (m s)$^{-1}$
R_{lam2}	1.53×10^7 (m s)$^{-1}$
R_{lam3}	1.43×10^6 (m s)$^{-1}$
K_{turb1}	47,940 (m kg)$^{-0.5}$
K_{turb2}	54,901 (m kg)$^{-0.5}$
K_{turb3}	44,651 (m kg)$^{-0.5}$

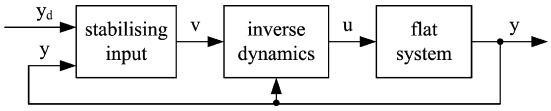

Fig. 10. Structure of the flatness-based control.

the system are given by the pressures at the capacities:

$$\underline{u} = \begin{bmatrix} \dot{m}_{MFC,d} \\ R_T \end{bmatrix}, \quad \underline{x} = \begin{bmatrix} p_1 \\ p_2 \\ p_3 \end{bmatrix}, \quad \underline{\tilde{y}} = \begin{bmatrix} p_2 \\ \lambda_{O_2} \end{bmatrix}. \tag{20}$$

As the system is nonlinear, flatness-based control techniques are envisaged.

5.1. Principles of flatness-based control

Differential flatness is a geometrically motivated concept for analysis and synthesis of nonlinear systems. According to Ref. [8], nonlinear flat systems are equivalent, in a more general way, to linear controllable systems (Fig. 10).

A system is denoted flat if an output vector $\underline{y} = [y_1, \ldots, y_p]^T$ exists that fulfills the following conditions:

(i) The output variables y_i can be stated as functions of the state variables x_i, the input variables u_i and a finite number of their time derivatives

$$\underline{y} = \underline{\Phi}(\underline{x}, \underline{u}, \dot{\underline{u}}, \ldots, \underline{u}^{(\alpha)}). \tag{21}$$

(ii) All state variables x_i and all inputs u_i can be stated as functions of the output variables y_i and a finite number of their time derivatives

$$\underline{x} = \underline{\Psi}_1(\underline{y}, \dot{\underline{y}}, \ldots, \underline{y}^{(\beta)}), \tag{22}$$

$$\underline{u} = \underline{\Psi}_2(\underline{y}, \dot{\underline{y}}, \ldots, \underline{y}^{(\beta+1)}). \tag{23}$$

(iii) The dimension of the input vector is equal to the dimension of the output vector

$$dim\,\underline{u} = dim\,\underline{y}. \tag{24}$$

If the output variables of interest can be proven flat outputs, trajectory tracking control design becomes straight-forward. The dynamics of the resulting linear error dynamics can be specified by introducing a new stabilising input

$$v_i = y_{i,d}^{(\beta+1)} + k_\beta(y_{i,d}^{\beta} - y_i^{\beta}) + \cdots + k_0(y_{i,d} - y_i) \tag{25}$$

and replacing the highest derivative of y_i in the expression of the control input with v_i according to (25). This results in the following inverse dynamics

$$\underline{u} = \underline{\Psi}_2(\underline{y}, \dot{\underline{y}}, \ldots, \underline{y}^{\beta}, \underline{v}), \tag{26}$$

where the control inputs are calculated depending on the measured and desired outputs.

5.2. Application to the system

For the proof of flatness the system description from Section 3.6 is examined. Unfortunately, the proof of the flat output candidate $\underline{\tilde{y}}$ according to (20) fails. Instead, it can be shown that $\underline{y} = [y_1\ y_2]^{\mathrm{T}} = [p_1\ u_{\mathrm{H_2}}]^{\mathrm{T}}$ represents a flat output. The desired value $p_{1,\mathrm{d}}$ for the inlet pressure can be derived from the steady-state values of the desired value $p_{2,\mathrm{d}}$ for the cathode pressure, the actual mass flow $\dot{m}_1$ and the flow resistance R_{I}

$$p_{1,\mathrm{d}} = p_{2,\mathrm{d}} + R_{\mathrm{I}}\,\dot{m}_1. \tag{27}$$

The actual values of the turbulent resistances are calculated by using the steady-state values of the according pressure differences. The relative degree of the first input y_1 is three, whereas for the second input y_2 the relative degree becomes one.

According to (25) and (26), the new stabilising input

$$\underline{v} = \begin{bmatrix} \dddot{y}_1 \\ \dot{y}_2 \end{bmatrix} = \begin{bmatrix} \dddot{y}_{1,\mathrm{d}} + k_{12}\,\ddot{e}_1 + k_{11}\,\dot{e}_1 + k_{10}\,e_1 \\ \dot{y}_{2,\mathrm{d}} + k_{20}\,e_2 \end{bmatrix} \tag{28}$$

is introduced and inserted into the inverse dynamics

$$\underline{u} = \begin{bmatrix} \dot{m}_{\mathrm{MFC,d}} \\ R_{\mathrm{T}} \end{bmatrix} = \begin{bmatrix} \Psi_{21}(y_1, \dot{y}_1, \ddot{y}_1, v_1, y_2, v_2) \\ \Psi_{22}(y_1, y_2, v_2) \end{bmatrix}. \tag{29}$$

Thus, the linear tracking error dynamics

$$\begin{aligned} &\dddot{e}_1 + k_{12}\,\ddot{e}_1 + k_{11}\,\dot{e}_1 + k_{10}\,e_1 = 0 \\ &\dot{e}_2 + k_{20}\,e_2 = 0, \end{aligned} \tag{30}$$

with $e_i = y_{i,\mathrm{d}} - y_i$ can be specified by the coefficients k_{12}, k_{11}, k_{10} and k_{20}.

6. Cathode pressure observation

The aim of the feedback control is to maintain a constant cathode pressure. However, the pressure p_2 at the electrode inside the fuel cell stack is a state variable that cannot be measured directly. The only measurable state variable is the pressure p_3 at the outlet throttle. Since the turbulent flow resistances increase with raising pressure, it is not advisable to control the output pressure p_3 instead of the cathode pressure p_2. Especially at high mass flows both pressures differ significantly (cf. Fig. 16). An alternative is to estimate the cathode pressure dynamically.

The fuel cell current is measured and therefore, the actual utilisation follows from Faraday's Law (1). The actual value of the inlet mass flow $\dot{m}_1$ is available from the MFC. The actual flow resistance R_{T} of the throttle is known as well. Under these preconditions the pressure p_2 at the electrode can be estimated by a tracking observer.

For the observer design the input u, the measured output y_{m} and the states $\underline{x}$ are chosen as follows

$$u = \dot{m}_1, \quad \underline{x} = [p_1, p_2, p_3]^{\mathrm{T}}, \quad y_{\mathrm{m}} = p_3 \tag{31}$$

and lead to the corresponding nonlinear state space description

$$\dot{\underline{x}} = \underline{f}(\underline{x}, u), \tag{32}$$

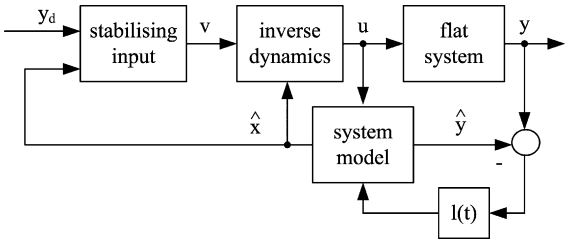

Fig. 11. Structure of the nonlinear tracking observer.

$$y = h(\underline{x}) = x_3. \tag{33}$$

Consequently, the flatness-based feedback control (29) can be realised with the estimated state vector $\underline{\hat{x}}$ provided by a nonlinear tracking observer

$$\dot{\underline{\hat{x}}} = \underline{f}(\underline{\hat{x}}, \hat{u}) + \underline{l}(t)\,(y_{\mathrm{m}} - h(\underline{\hat{x}})), \tag{34}$$

with time-varying observer-gain $\underline{l}(t)$ [8] (Fig. 11).

The derivation of the observer-gain is discussed in detail in Ref. [3]. For the air supply system the time-varying observer-gain results in

$$\underline{l}(t) = [l_1(t), l_2(t), l_3(t)]^{\mathrm{T}}, \tag{35}$$

where all components depend on the pressure dependent turbulent resistances and the third gain additionally on the actual throttle resistance R_{T}.

7. Simulation results

In the following, the effectiveness of the proposed nonlinear multivariable control combined with the observer is investigated by simulations, where the fuel cell current acts as disturbance on the fuel cell system. The current variation is given by a sequence consisting of a steep increase from 0.1 A $\mathrm{cm}^{-2}$to 0.4 A cm^{-2}, a subsequent constant level of 0.4 A cm^{-2}, and a steep decline to 0.1 A cm^{-2} as shown in Fig. 12.

The resulting time response of the control outputs, i.e., the excess ratio of oxygen $\lambda_{\mathrm{O_2}}$ and the cathode pressure p_2, are depicted in Figs. 13 and 14, respectively.

During steady-state, both excess ratio of oxygen $\lambda_{\mathrm{O_2}}$ and the cathode pressure p_2 match their desired values. At the rising

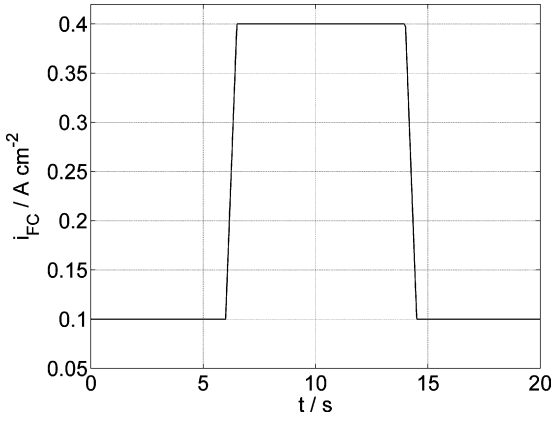

Fig. 12. Fuel cell current.

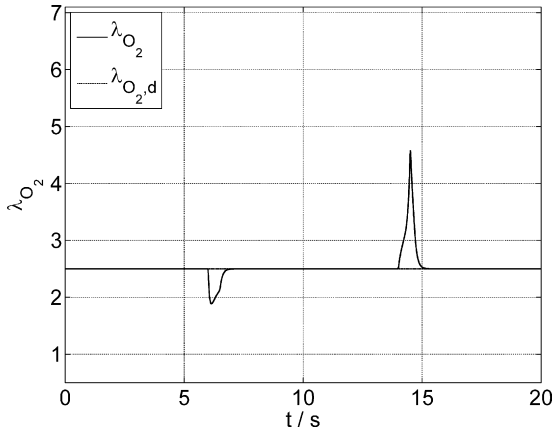

Fig. 13. Excess ratio of oxygen λ_{O_2} using observer-based multivariable control.

edge, the excess ratio reaches a minimum of 1.9 and a maximum of 4.6 at the falling edge. Since the excess ratio never falls below 1, the fuel cell is never in danger of starvation. Due to the increase in current it is expected that the pressure level at the cathode decreases. But as can be seen in Fig. 14, p_2 increases slightly from 5×10^4 to 5.15×10^4 Pa. This has to be seen in the context that p_1 is controlled with the input variables in (29). Due to diffusion effects through the gas diffusion layer the occurring pressure increase in the cathode is advantageous at rising currents.

The observed values of the cathode pressure $\hat{p}_2$ follow the simulated values with high accuracy. The corresponding observer error $e_{o,p_2} = \hat{p}_2 - p_2$ of the anode pressure is depicted in Fig. 15.

To emphasise the effectiveness of the proposed flatness-based control extended with the nonlinear tracking observer, a comparison with the commonly used combination of feedforward control of the mass flow $\dot{m}_{MFC}$ and PI-control of the outlet pressure p_{out} at the outlet throttle has been performed. Here, the same current trajectory as depicted in Fig. 12 has been employed.

Since the outlet pressure p_{out} is controlled instead of p_2, the cathode pressure is subject to steady-state error, especially at high current densities (cf. Fig. 16). At the first load change the cathode pressure drops and at the second load change to lower

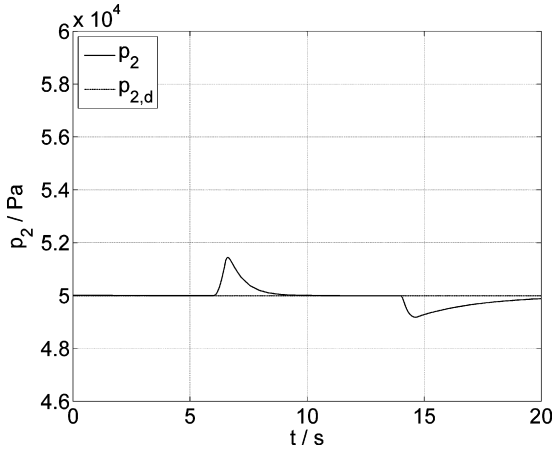

Fig. 14. Cathode pressure p_2 using observer-based multivariable control.

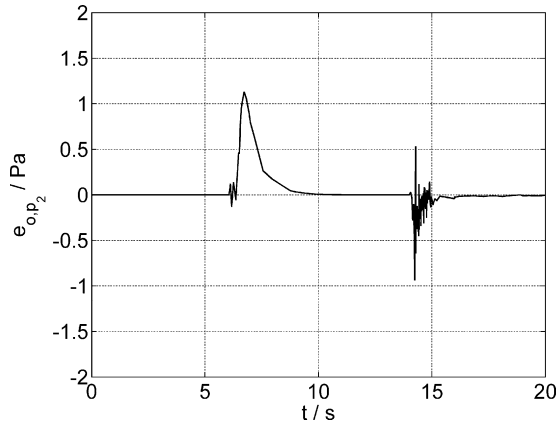

Fig. 15. Observer error of the cathode pressure.

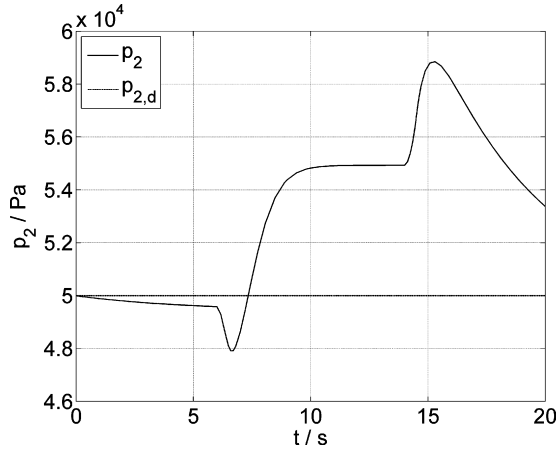

Fig. 16. Cathode pressure p_2 with the commonly used PI-control of the outlet pressure p_{out}.

current values a peak pressure is observed inside the fuel cell stack.

The feedforward controlled excess ratio of oxygen reaches values close to 1 at the rising edge of the current trajectory (cf. Fig. 17). For this period, the fuel cell runs the risk of starvation.

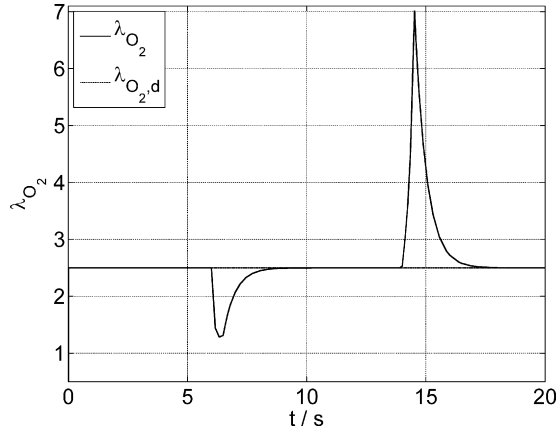

Fig. 17. Excess ratio of oxygen λ_{O_2} with the commonly used feedforward control of the mass flow.

8. Conclusion and outlook

As basis for both control and observer design, a dynamic model of the air supply subsystem at the cathode side of the fuel cell is derived. The control objectives in terms of obtaining high overall efficiency and avoiding starvation are achieved by multivariable control of both cathode pressure and excess ratio of oxygen. With the designed control structure the fuel cell system can be operated dynamically at lower excess ratios of oxygen without running the risk of starvation. The non-measurable anode pressure is estimated by a nonlinear tracking observer. The dynamic pressure observer allows for detecting pressure drops and peak pressures in the cathode volume and, thereby, reduces the danger of starvation and overpressure, respectively.

The effectiveness of the control system is shown by comparing the simulation results of the proposed nonlinear control structure with the results of a usually used feedforward control of the mass flow combined with a PI-control of the outlet pressure. At this, the same current trajectory is employed.

Future work envisages a system where the MFC is replaced by a compressor. In the model the dynamics of the MFC is substituted by a model of the compressor dynamics. Finally, an air supply system is obtained with two voltages as control variables, one for the compressor and the second for the outlet throttle. To realise the same multivariable control and observer design as discussed above two pressure sensors are sufficient: one at the outlet of the compressor to determine the mass flow into the system and the second, as hitherto, at the outlet throttle.

To further minimise the danger of starvation the developed control system can be extended by a load governor [11]. Thereby, the current drawn from the fuel cell can be constricted depending on the observed pressure at the electrodes, so that the constraint on the oxygen partial pressure inside the cathode is strictly enforced.

Acknowledgement

The authors gratefully acknowledge the cooperation and support by the centre for solar energy and hydrogen research (ZSW) in Ulm, especially for their assistance in setting up the test rig and for providing the fuel cell stack.

References

[1] J. Amphlett, R. Baumert, R. Mann, B. Peppley, P. Roberge, J. Electrochem. Soc. 142 (1) (1995) 9–15.
[2] K. Dannenberg, P. Ekdunge, G. Lindbergh, J. Appl. Electrochem. 30 (2000) 1377–1387.
[3] M.A. Danzer, H. Aschemann, E.P. Hofer, Proceedings of 12th IEEE International Conference on Methods and Models in Automation and Robotics, Miedzyzdroje, Poland, 2006.
[4] H. Dubbel, Taschenbuch für den Maschinenbau, vol. 17, Springer, 1990 (in German).
[5] J. Nelder, R. Mead, Comput. J. 7 (1965) 308–313.
[6] J.T. Pukrushpan, H. Peng, A.G. Stefanopoulou, Proceedings of IMECE'02, International Mechanical Engineering Congress & Exposition, 2002.
[7] J.T Pukrushpan, A.G. Stefanopoulou, H. Peng, Control Syst. Mag. 24 (2004) 30–46.
[8] R. Rothfuß, J. Rudolph, M. Zeitz, Automatisierungstechnik 45 (1997) 517–525.
[9] H.M. Schaedel, Fluidische Bauelemente und Netzwerke, Vieweg, 1979 (in German).
[10] G. Schmidt, Grundlagen der Regelungstechnik, Springer, 1991 (in German).
[11] J. Sun, I. Kolmanovsky, Proceedings of the 2004 American Control Conference, Boston, Massachussetts, 2004, pp. 828–833.
[12] A. Vahidi, A. Stefanopoulou, H. Peng, Proceedings of the American Control Conference, 2004.
[13] J. Wilhelm, Modellierung, Identifikation und Regelung der kathodenseitigen Gaszufuhr einer PEM-Brennstoffzelle, Diploma Thesis, Ulm University, 2005 (in German).